

## ORIGINAL ARTICLE

# *Ppp6c* haploinsufficiency accelerates UV-induced BRAF(V600E)-initiated melanomagenesis

Kosuke Kanazawa<sup>1,2,3</sup> | Kazuhiro Kishimoto<sup>1,3,4</sup> | Miyuki Nomura<sup>1</sup> |  
 Koreyuki Kurosawa<sup>1,5</sup> | Hiroyuki Kato<sup>1</sup> | Yui Inoue<sup>1</sup> | Koh Miura<sup>2</sup> | Katsuya Fukui<sup>1,3</sup> |  
 Yoji Yamashita<sup>1</sup> | Ikuro Sato<sup>6</sup> | Hiroyuki Tsuji<sup>4</sup> | Toshio Watanabe<sup>7</sup> | Takuji Tanaka<sup>8</sup> |  
 Jun Yasuda<sup>3,9,10</sup> | Nobuhiro Tanuma<sup>1,3</sup>  | Hiroshi Shima<sup>1,3</sup> 

<sup>1</sup>Division of Cancer Chemotherapy, Miyagi Cancer Center Research Institute, Miyagi, Japan

<sup>2</sup>Division of Surgery, Miyagi Cancer Center, Miyagi, Japan

<sup>3</sup>Division of Cancer Molecular Biology, Tohoku University School of Medicine, Miyagi, Japan

<sup>4</sup>Department of Head and Neck Surgery, Kanazawa Medical University, Ishikawa, Japan

<sup>5</sup>Department of Plastic and Reconstructive Surgery, Tohoku University School of Medicine, Miyagi, Japan

<sup>6</sup>Division of Pathology, Miyagi Cancer Center, Miyagi, Japan

<sup>7</sup>Department of Biological Science, Graduate School of Humanities and Sciences Nara Women's University, Nara, Japan

<sup>8</sup>Research Center of Diagnostic Pathology, Gifu Municipal Hospital, Gifu, Japan

<sup>9</sup>Cancer Genome Center, Miyagi Cancer Center Research Institute, Miyagi, Japan

<sup>10</sup>Tohoku Medical Megabank Organization, Tohoku University, Miyagi, Japan

**Correspondence**

Hiroshi Shima, Division of Cancer Chemotherapy, Miyagi Cancer Center Research Institute, 47-1 Nodayama, Medeshima-Shiode, Natori, Miyagi, 981-1293 Japan.  
 Email: shima@med.tohoku.ac.jp

**Funding information**

JSPS KAKENHI, Grant/Award Number: 19K18757, 18K16043 and 17K07187

**Abstract**

According to TCGA database, mutations in *PPP6C* (encoding phosphatase PP6) are found in c. 10% of tumors from melanoma patients, in which they coexist with *BRAF* and *NRAS* mutations. To assess PP6 function in melanoma carcinogenesis, we generated mice in which we could specifically induce BRAF(V600E) expression and delete *Ppp6c* in melanocytes. In these mice, melanoma susceptibility following UVB irradiation exhibited the following pattern: *Ppp6c* semi-deficient (heterozygous) > *Ppp6c* wild-type > *Ppp6c*-deficient (homozygous) tumor types. Next-generation sequencing of *Ppp6c* heterozygous and wild-type melanoma tumors revealed that all harbored *Trp53* mutations. However, *Ppp6c* heterozygous tumors showed a higher Signature 1 (mitotic/mitotic clock) mutation index compared with *Ppp6c* wild-type tumors, suggesting increased cell division. Analysis of cell lines derived from either *Ppp6c* heterozygous or wild-type melanoma tissues showed that both formed tumors in nude mice, but *Ppp6c* heterozygous tumors grew faster compared with those from the wild-type line. *Ppp6c* knockdown via siRNA in the *Ppp6c* heterozygous line promoted the accumulation of genomic damage and enhanced apoptosis relative to siRNA controls. We conclude that in the presence of BRAF(V600E) expression and UV-induced *Trp53* mutation, *Ppp6c* haploinsufficiency promotes tumorigenesis.

**KEYWORDS**

BRAF, haploinsufficiency, melanoma, protein phosphatase 6, UV-induced carcinogenesis

This is an open access article under the terms of the Creative Commons Attribution-NonCommercial-NoDerivs License, which permits use and distribution in any medium, provided the original work is properly cited, the use is non-commercial and no modifications or adaptations are made.

© 2021 The Authors. *Cancer Science* published by John Wiley & Sons Australia, Ltd on behalf of Japanese Cancer Association.

## 1 | INTRODUCTION

Melanoma is the most aggressive and, until recently, the most treatment-resistant form of skin cancer. Recent sequencing analyses of melanoma tumors have also identified tumor-specific genes, further altering treatment approaches.<sup>1</sup> For example, sequencing screens of melanoma cells have revealed several recurrently mutated genes, including in *Ppp6c*, which encodes protein phosphatase 6 (PP6).<sup>2,3</sup> *Ppp6c* somatic mutations are reported in 12% of sun-exposed malignant melanoma cases, exclusively in tumors with *BRAF* or *NRAS* mutations. Moreover, *Ppp6c* mutations often occur in genomic hot spots associated with protein function or stability,<sup>3,4</sup> suggesting that *Ppp6c* loss is associated with tumor formation.

PP6 associates with 3 regulatory proteins, PP6R1, PP6R2, and PP6R3, which regulate its localization and substrate specificity.<sup>5-7</sup> In mammalian cell lines, diverse phenotypes seen following siRNA-based *Ppp6c* depletion suggest that PP6 plays an important role in several cancer-relevant pathways, including DNA damage repair via activation of DNA-PK,<sup>8,9</sup> mitosis regulation by Aurora A dephosphorylation,<sup>10</sup> and anti-inflammation by suppression of NFκB signaling.<sup>11-13</sup> Moreover, pathological data suggest that PP6 is down-regulated in several cancers. For example, in human breast cancers, PP6, PP6R1, PP6R2, and PP6R3 protein levels decrease.<sup>14</sup> *MIR-373*, a tumor-promoting microRNA that targets *Ppp6c*, is overexpressed in various tumor types, including esophageal squamous cell carcinoma<sup>15</sup> and hepatocellular carcinoma,<sup>16</sup> potentially accounting for why *mir-373* expression increases cell proliferation in both tumor types. Overall, these data suggest that *Ppp6c* functions as a tumor suppressor in some cancer contexts.

We previously examined *Ppp6c* function in vivo using a non-melanoma skin carcinogenesis mouse model in which *Ppp6c* was deleted following Cre induction in cytokeratin 14-positive keratinocytes. *Ppp6c*-deficient keratinocytes were predisposed to DMBA-induced papilloma formation<sup>17</sup> and UV-induced squamous cell carcinoma formation.<sup>18</sup> Recently, we observed that *Ppp6c* deficiency enhances *K-ras*<sup>G12D</sup>-dependent tumor promotion in keratinocytes.<sup>19</sup> These results indicate that, in these contexts, *Ppp6c* suppresses skin carcinogenesis. However, it remained unknown whether *Ppp6c* functioned similarly in the context of melanoma.

*Ppp6c* loss-of-function mutations are reportedly present in UV-induced melanoma tissue, in which they coexist with activating mutations in *BRAF* or *NRAS*, but not with *PTEN* mutation, suggesting that, in melanoma development, PP6 is anti-oncogenic in the context of mutant *BRAF* or *NRAS*, as is *PTEN*. Here, to assess the effects of PP6 loss on activated *BRAF*-induced melanomagenesis, we used a system in which the Cre-Activated/CA allele of *BRAF* is converted to the oncogenic *BRAF*<sup>V600E</sup>/VE allele<sup>20</sup> following Cre-based recombination in melanocytes. Using this system in mice on either a *Ppp6c*-deficient or semi-deficient background, we assessed the effects of *Ppp6c* loss on UVB-induced-, *BRAF*(V600E)-initiated melanomagenesis. We report that mice with 1 functional *Ppp6c* allele are more susceptible to

UVB-induced *BRAF*(V600E)-initiated melanomagenesis than are comparable *Ppp6c* null or *Ppp6c* wild-type (WT) mice.

## 2 | MATERIALS AND METHODS

### 2.1 | Generation of mice exhibiting melanocyte-specific inducible *BRAF*<sup>V600E</sup> and *Ppp6c* deletion

*Tyr-CreER*<sup>T2</sup>:*BRAF*<sup>CA/CA</sup>:*Ppp6c*<sup>flox/+</sup> mice were generated by breeding siblings obtained by crossing between *Tyr-CreER*<sup>T2</sup>:*BRAF*<sup>CA</sup>:*Pten*<sup>loxP</sup> (Jackson Laboratory 013 590) with *Ppp6c*-floxed (*Ppp6c*<sup>flox/flox</sup>) mice, as reported previously.<sup>21</sup> *Tyr-CreER*<sup>T2</sup>:*BRAF*<sup>CA/+</sup>:*Ppp6c*<sup>flox/flox</sup>, *Tyr-CreER*<sup>T2</sup>:*BRAF*<sup>CA/+</sup>:*Ppp6c*<sup>flox/+</sup>, or *Tyr-CreER*<sup>T2</sup>:*BRAF*<sup>CA/+</sup>:*Ppp6c*<sup>+/+</sup> mice used here were obtained by mating *Tyr-CreER*<sup>T2</sup>:*BRAF*<sup>CA/CA</sup>:*Ppp6c*<sup>flox/+</sup> with *Ppp6c*<sup>flox/+</sup> mice. All animal experiments were performed with the approval of the Miyagi Cancer Center Research Institute Animal Care and Use committee (MCCAE-2020-1).

### 2.2 | Reagents

4-Hydroxytamoxifen (4HT) was purchased from Toronto Research Chemicals (North York, Canada).

### 2.3 | UVB induction of melanomagenesis

The dorsal skin of 8-wk-old mice generated as described above was shaved and then treated daily for 3 d with 100 μL acetone containing 4HT (25 mg/ml). At 2 wk after the first treatment, mice were anesthetized with isoflurane and subjected to 1 min of 2 kJ/m<sup>2</sup> UVB irradiation once a week for 6 mo using a Bio-Link BLX system (Vilber Lourmat, France). The spectral peak of the UVB source was 312 nm. The number of tumors exceeding 1 mm in diameter was evaluated weekly.

### 2.4 | Histopathology and immunohistochemistry

Mouse tissues exhibiting subcutaneous tumors were dissected, fixed overnight in buffered 10% neutral formalin at room temperature, transferred to sequential 70%, 80%, 90% and 100% methanol washes, and embedded in paraffin. Sections were stained with H&E and examined microscopically by 2 pathologists. Most tumors were histopathologically hypomelanotic, but melanoma-like. Therefore, histopathological diagnosis was conducted based on criteria described for human malignant melanoma<sup>22-25</sup> after immunohistochemical analysis<sup>26</sup> with the following antibodies: rabbit antibody against mouse Ki67 (#9449 Cell Signaling Technology Inc, Danvers, USA); rabbit antibody against mouse S100 (#ab183979, Abcam Inc, Cambridge UK); rabbit antibody against mouse SOX10 (#ab108408, Abcam Inc); and mouse antibody against mouse HMB45(#M0634 DAKO, Glostrup, Denmark).

## 2.5 | Tumorigenicity test

For allograft experiments, melanoma cells were injected subcutaneously into the dorsal flank of nude mice at  $1 \times 10^6$  cells per injection site. Tumor length and width were measured using calipers, and tumor volume was calculated based on the standard formula ( $\text{length} \times \text{width}^2/2$ ).

## 2.6 | Isolation and culture of melanoma cells

Melanoma cells were isolated and cultured using the method of Soo.<sup>27</sup> In brief, when tumor volume reached 2000 mm<sup>3</sup>, mice were euthanized and tumors were collected. After rinsing in PBS, tumors were incubated in 1.5 ml PBS plus 1.5 ml trypsin-EDTA solution (Sigma-Aldrich, St Louis, MO) at 37°C for 15 min, and then 10 ml of RPMI growth medium containing 5% FCS was added. The cell suspension was passed through a cell strainer (100  $\mu\text{m}$ : Falcon #354 360) and then plated onto mitomycin-treated XB2 keratinocytes and cultured in RPMI growth medium containing 5% FCS with 200 nM TPA. After cells were maintained 1 mo, they were stocked for later use in transplantation experiments or for in vitro analysis.

## 2.7 | RNAi analyses

Cells were transfected with siRNA using Lipofectamine RNAiMAX Transfection Reagent (Thermo Fisher Scientific, Waltham, MA). siRNAs used were: SMART pool siGENOME mouse *Ppp6c* siRNA and ON-TARGET plus Non-targeting siRNA#1 (Dharmacon, Lafayette, CO).

## 2.8 | Western blot analyses

Cells were lysed by sonication in RIPA buffer (50 mM Tris-Cl, 150 mM NaCl, 1 mM EDTA, 0.1% SDS, 1% Triton-X100 and 10% glycerol) supplemented with protease and phosphatase inhibitor cocktails and cleared by centrifugation at 14 000 rpm for 10 min at 4°C. Protein concentrations were determined using a DC protein assay (Bio-Rad, Hercules, CA), and then equal amounts of protein were subjected to SDS-PAGE using a 4%-20% Mini Gel (Bio-Rad). Proteins were transferred onto PVDF membranes using the Trans-Blot Turbo Transfer System (Bio-Rad), and membranes were blocked at room temperature with skimmed milk in PBS/Tween buffer. Immunoblot staining was performed in accordance with standard procedures using Western Lightning Plus-ECL (PerkinElmer, Waltham, MA) as detection reagent. Antibodies used were: anti-PP6 polyclonal antibody,<sup>17</sup> anti-caspase-3 polyclonal antibody (#9662, Cell Signaling Technologies, Danvers, MA), anti-cleaved caspase-3 polyclonal antibody (#9661, Cell Signaling Technologies), anti- $\gamma$ H2AX monoclonal antibody (#05-636, Merck, Kenilworth, NJ) and anti- $\beta$ -actin HRP monoclonal antibody (PM053-7, MBL, Nagoya, Japan).

## 2.9 | Analysis of cell proliferation

An in vitro Toxicology Assay Kit, sulforhodamine B based (Sigma-Aldrich) was used to assess the effects of *Ppp6c* knockdown on cell proliferation, in accordance with the manufacturer's protocol.

## 2.10 | Target selection and sequencing

We outsourced whole exome sequencing analyses to Riken Genesis (Kawasaki, Japan). Genomic DNA was extracted from formalin-fixed paraffin-embedded (FFPE) tissue using a GeneRead DNA FFPE kit (Promega, Madison, WI), sheared into c. 200 bp fragments, and used to construct a library for multiplexed paired-end sequencing with the SureSelect<sup>XT</sup> Reagent Kit (Agilent Technologies, Santa Clara, CA). The library was hybridized to biotinylated cRNA oligonucleotide baits from the SureSelect<sup>XT</sup> Mouse All Exon Kit (cat no. 5180-4641, Agilent Technologies) for target enrichment. Targeted sequences were purified by magnetic beads, amplified, and sequenced on an Illumina NovaSeq 6000 platform in a paired-end 151 bp configuration.

## 2.11 | Mapping and SNV/InDel calling

Basic bioinformatics analyses from pre-processing to variant filtrations were outsourced to Riken Genesis. Briefly, adapter sequences were removed using cutadapt (v.1.2.1). After quality control, reads were mapped to the reference mouse genome (mm10) using BWA (v.0.7.10). Mapping results were corrected using Picard (v.1.73) to remove duplicates and subjected to GATK analysis (v.1.6-13) for local alignment and quality score recalibration. SNV and InDel calls were performed with multi-sample calling using GATK, and filtered to coordinates with VQSR (Variant Quality Score Recalibration) passed and a variant call quality score  $\geq 30$ . Annotations of SNVs and InDels were based on dbSNP150, CCDS (NCBI, Release 21), RefSeq (UCSC Genome Browser, Nov. 2018), and Gencode (UCSC Genome Browser, v.M18) analyses. Variants with following predicted functions were selected for further analyses: frameshift, nonsense, read-through, missense, deletion, insertion, or insertion-deletion.

## 2.12 | Bioinformatics

Variants were further filtered to remove less reliable and/or potential germline samples. To do so, we removed variants that genotyped fewer than 8 samples among the 15. We then removed variants found in multiple samples as potential polymorphisms. Remaining variants are summarized in Table 2.

For mutant signature analyses, we removed small InDels. Mutational signature analyses were conducted with deconstructSigs software.<sup>28</sup> Relevant to *Trp53* mutation depth, we obtained the number of reads from VCF files and checked data manually using

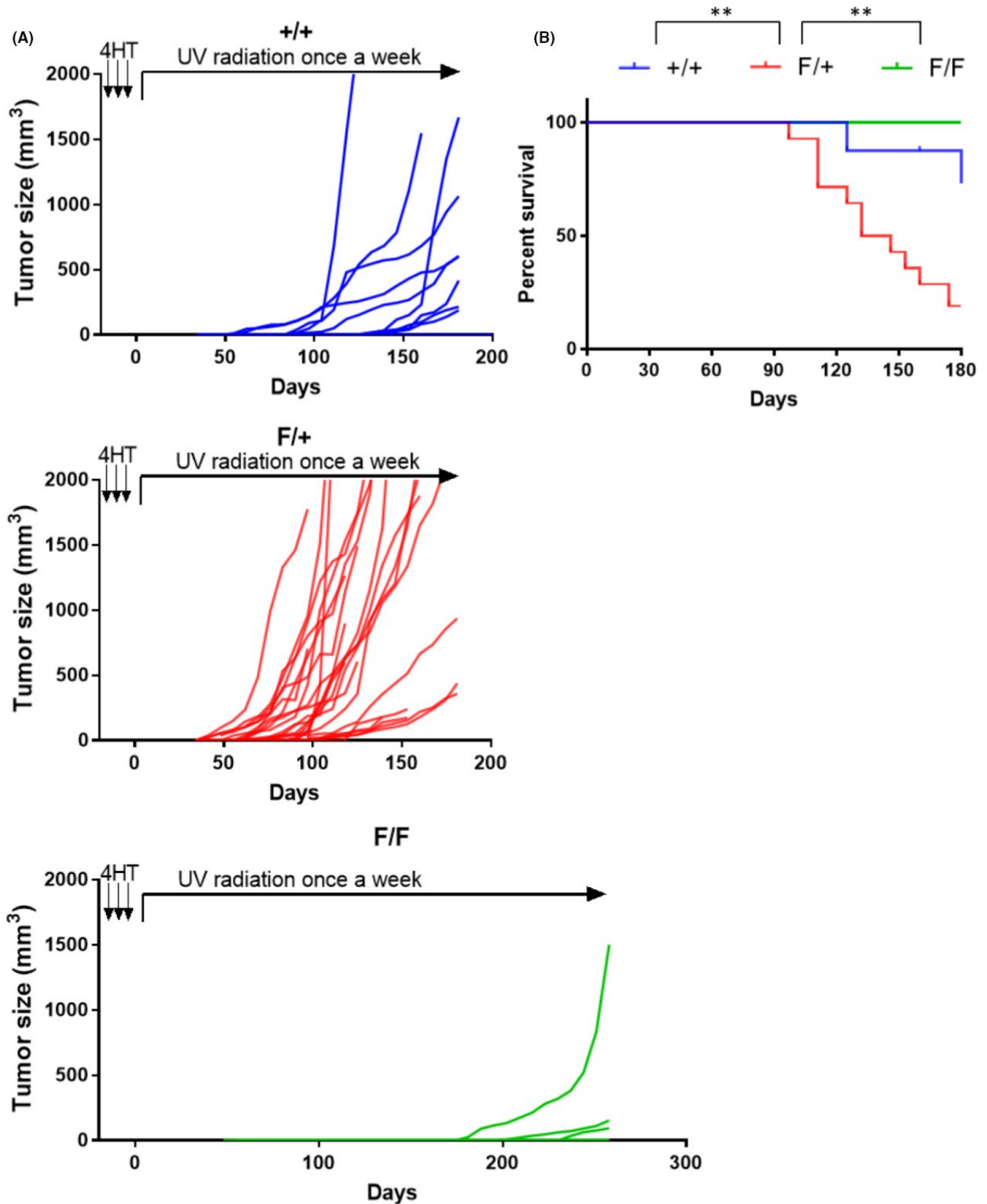


**FIGURE 1** *Ppp6c* haploinsufficiency accelerates melanocyte tumorigenesis in UVB-induced carcinogenesis. A, At 2 wk after 4HT treatment, *Tyr-CreER<sup>T2</sup>:BRAF<sup>CA/+</sup>* mice that also harbor either WT (+/+) *Ppp6c* (top; n = 8), or heterozygous (F/+) (middle; n = 14), or homozygous (F/F) (bottom; n = 7) *Ppp6c* mutations were UVB-irradiated once a week at a dose of 2 KJ/m<sup>2</sup>. Shown is tumor growth rate in respective groups. B, Percent of mice surviving in indicated groups. \*\**P* < .01

Integrative Genome Viewer.<sup>29</sup> Comparison of human and mouse *Trp53* mutations was undertaken as follows. First, we aligned mouse *Trp53* mutations to human genome positions using command line LiftOver software.<sup>30</sup> We then generated potential human *TP53* mutation patterns with single nucleotide replacement at those positions. Then, using annovar<sup>31</sup> we annotated possible *TP53* mutations with COSMIC database v.90<sup>32</sup> and picked up the same amino acid changes corresponding to mouse *Trp53* mutations identified in this study. Finally, we visualized the 8 *TP53* mutations with mutation mapper at the cBioPortal.<sup>33,34</sup>

## 2.13 | Statistical analysis

Kaplan-Meier survival curves and corresponding statistical analysis, as well as log-rank (Mantel-Cox) tests, were performed using Prism v.8 (GraphPad Software Inc, San Diego, California, USA). Other statistical significance was determined using Student *t* test. *P* < .05 served as the cut-off for significance.

## 3 | RESULTS

### 3.1 | UVB-induced melanomas in *Tyr-CreER<sup>T2</sup>:BRAFC<sup>CA/+</sup>:Ppp6c<sup>flox/+</sup>* mice

To determine the effect of *Ppp6c* genotype on melanoma development, we simultaneously induced BRAF(V600E) expression and changes in *Ppp6c* genotype in mouse melanocytes. To do so, we applied 4HT as inducer to various skin sites (back, abdomen, tail, and palm) of mice of 3 genotypes: *Tyr-CreER<sup>T2</sup>:BRAFC<sup>CA/+</sup>:Ppp6c<sup>+/+</sup>*, *Tyr-CreER<sup>T2</sup>:BRAFC<sup>CA/+</sup>:Ppp6c<sup>flox/+</sup>*, or *Tyr-CreER<sup>T2</sup>:BRAFC<sup>CA/+</sup>:Ppp6c<sup>flox/flox</sup>*. Over the next year, we observed no tumor development at any site in any genotype (data not shown). As previous publications indicate that *Ppp6c* mutations in human melanoma seen in tissues are likely to be sun-exposed,<sup>2,3</sup> we next used these models to assess the effects of exposure to UV light in mice expressing BRAF<sup>V600E</sup> plus various *Ppp6c* mutations. To do so, we again applied 4HT to the back skin of mice harboring 1 of the 3 genotypes described above, but then 2 wk later shaved these areas and subjected them to UVB irradiation once a week. We then monitored potential tumor formation for up to 180 d (Figure 1A). At a median of 102 d, 7 of 8 *Tyr-CreER<sup>T2</sup>:BRAFC<sup>CA/+</sup>:Ppp6c<sup>+/+</sup>* (+/+) mice exhibited melanomas (10 tumors in total) (Figure 1A, top), while at a median of 75 d 14 of 14 *Tyr-CreER<sup>T2</sup>:BRAFC<sup>CA/+</sup>:Ppp6c<sup>flox/+</sup>* (F/+) mice exhibited tumors (24 total) (Figure 1A, middle). Finally, in 7 *Tyr-CreER<sup>T2</sup>:BRAFC<sup>CA/+</sup>:Ppp6c<sup>flox/flox</sup>* (F/F) mice, we detected no tumor development for up to 180 d. When we continued to UVB-irradiate *Ppp6c<sup>flox/flox</sup>* type mice weekly for up to 260 d, 3 of 7 mice developed 1 tumor each (Figure 1A, bottom).

We monitored tumor size in each mouse and euthanized mice when tumors reached 2000 mm<sup>3</sup>. Figure 1B shows Kaplan-Meier survival curves up to 180 d for the 3 mouse groups genotypically *Tyr-CreER<sup>T2</sup>:BRAFC<sup>CA/+</sup>* plus either WT *Ppp6c* (+/+), heterozygous *Ppp6c*

(F/+), or *Ppp6c null* (F/F). *Ppp6c* heterozygotes (F/+) showed a statistically significant shorter survival time relative to either *Ppp6c* WT (*P* = .006) or null (*P* = .0015) mice.

Hypomelanotic subcutaneous tumors from 4HT-induced *Tyr-CreER<sup>T2</sup>:BRAFC<sup>CA/+</sup>* mice harboring WT *Ppp6c* resembled melanoma variants based on histopathological and immunohistochemical findings. Similarities included epithelioid, spindle cell, and pleomorphic types. However, tumors from comparable *Ppp6c* heterozygotes were spindle cell, desmoplastic, neurotropic, and pleomorphic types (Table 1). Moreover, tumors from *Ppp6c* null mice were spindle cell and desmoplastic types (data not shown).

We then confirmed recombination of BRAF<sup>CA</sup> and *Ppp6c<sup>flox</sup>* alleles in tumors from all 3 genotypes. Figure 2B shows representative PCR analysis of tumor #10 shown in Table 1. Recombination of the BRAF<sup>CA</sup> allele to BRAF<sup>VE</sup> initiated BRAF(V600E) expression from that allele, while recombination of the *Ppp6c<sup>flox</sup>* allele indicated loss of *Ppp6c* expression. We observed recombination of both in all 15 melanoma samples described in Table 1.

We next performed analysis of representative tumors. Figure 2A shows images of representative *Tyr-CreER<sup>T2</sup>:BRAFC<sup>CA/+</sup>:Ppp6c<sup>flox/+</sup>* mice bearing tumors #10 or #14 (see Table 1). Tumor #10 was histopathologically diagnosed as an epithelioid type of melanoma-like tumor, exhibiting histologic properties similar to human pigmented epithelioid melanoma.<sup>35</sup> Immunohistochemically, neoplastic cells in tumor #10 were strongly S100-positive (Figure 2C), although a few cells from this tumor were weakly positive for SOX10 and HMB45 (data not shown). Similarly, most cells in tumor #14, which was diagnosed as a desmoplastic type melanoma-like tumor,<sup>36</sup> were S100-positive (Figure 2C), as was

**TABLE 1** Genotype, histopathology, and immunohistochemistry of melanoma-like tumors

# tumor	<i>Ppp6c</i>	Histologic type	Ki67	S100
1	+/+	epithelioid type	+	+++
2	+/+	spindle cell type	+	++
3	+/+	desmoplastic type	+	++
4	+/+	spindle cell type	+	++
5	F/+	neurotropic type	+	+
6	F/+	neurotropic type	+	+
7	F/+	neurotropic type	+	+
8	F/+	spindle cell type	+	++
9	F/+	spindle cell type	+	++
10	F/+	epithelioid type	+	+++
11	F/+	neurotropic type	+	+
12	F/+	neurotropic type	+	+
13	F/+	pleomorphic type	++	+
14	F/+	desmoplastic type	+	++
15	F/+	neurotropic type	+	+

Note: Tumor cell immunopositivity was assigned 3 positive scores based on anti-Ki67 and anti-S100 staining. +, ++, or +++ indicated that respectively, 5%-20%, 20%-60%, or > 60% were positive for the indicated staining.

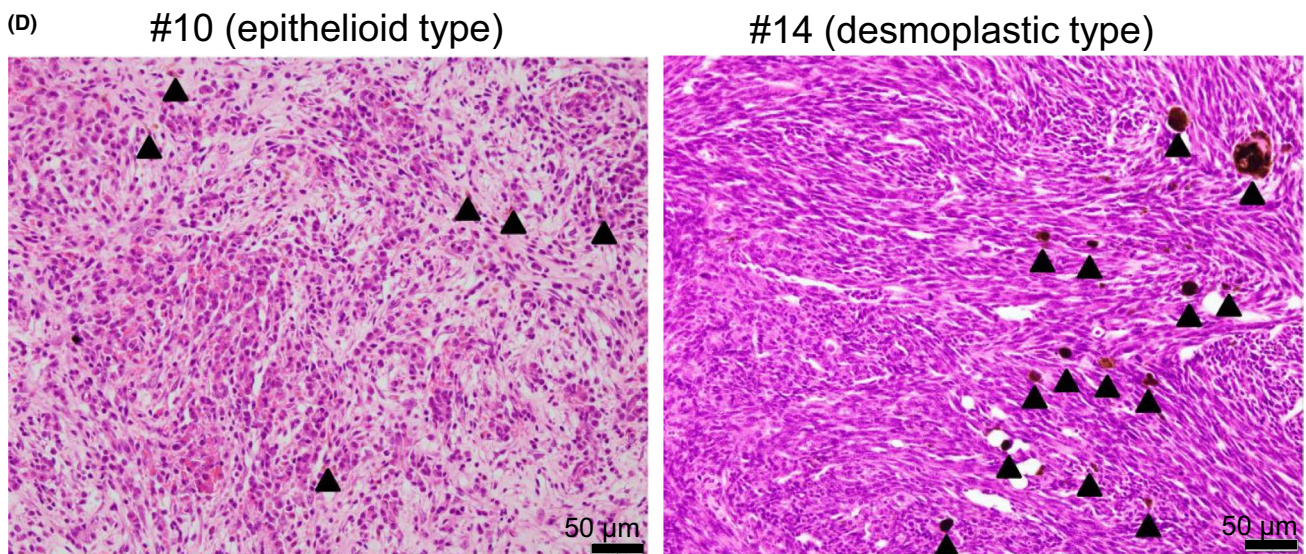
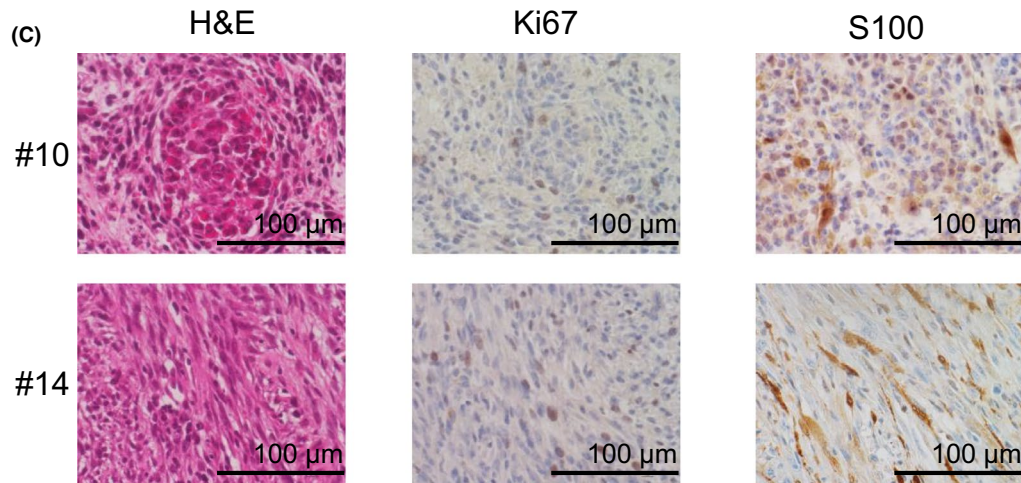
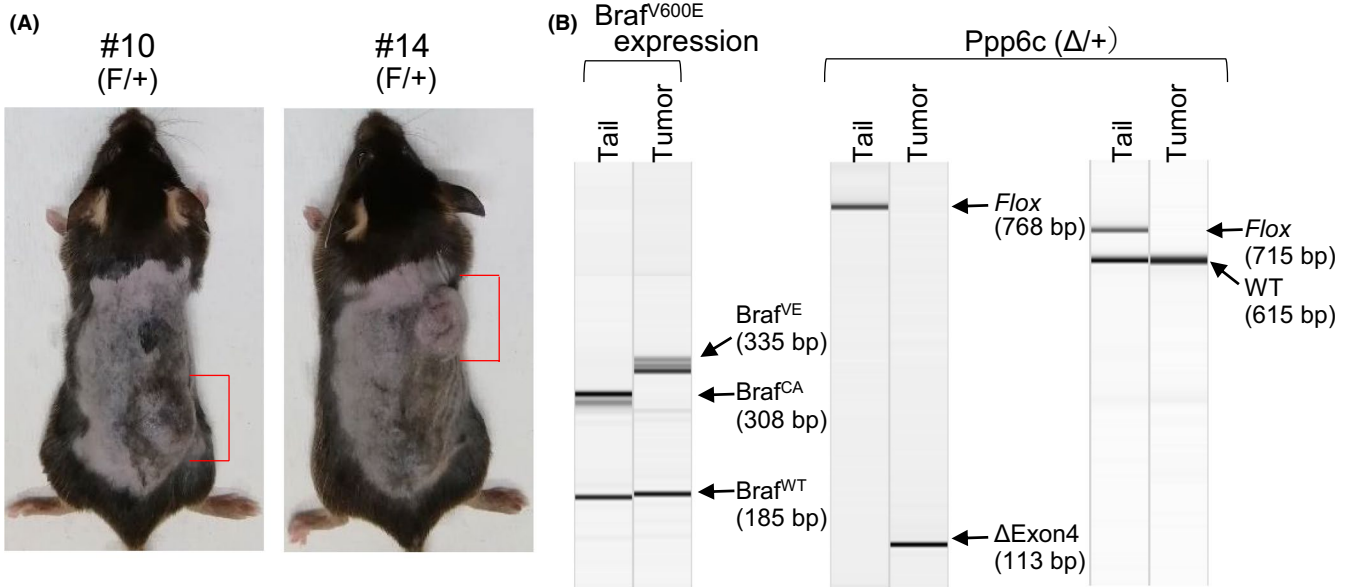
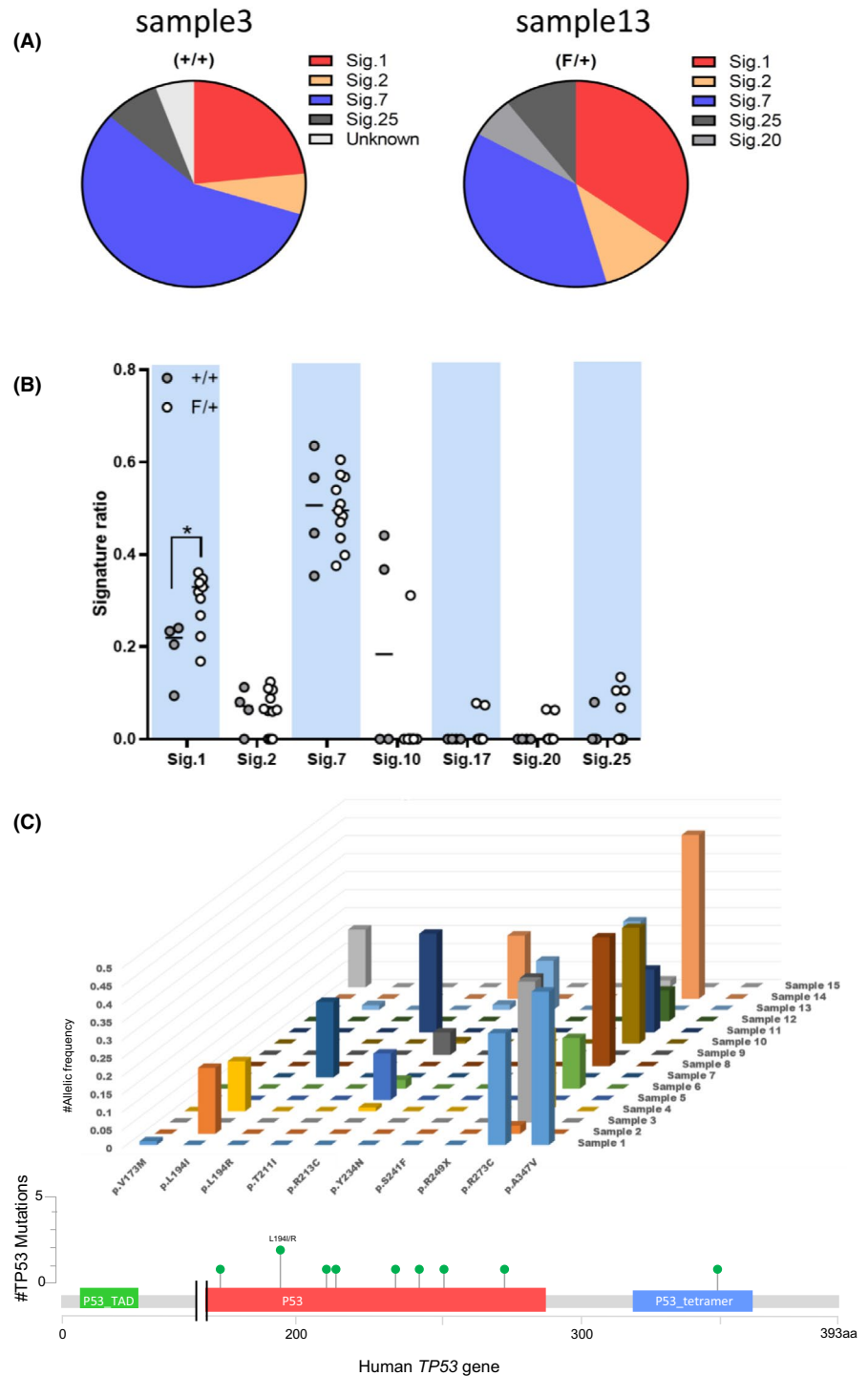


**FIGURE 2** UV-induced melanoma tumors in *Tyr-CreER<sup>T2</sup>:BRAF<sup>CA/+</sup>* mice heterozygous for *Ppp6c* (*Ppp6c<sup>flox/+</sup>*), and recombination of *BRAF* and *Ppp6c*-floxed alleles. A, Macroscopic appearance of representative (#10 and #14 in Table 1) tumors. Red brackets indicate areas exhibiting tumors. Both #10 and #14 are *Ppp6c* heterozygotes. B, PCR analysis of genomic DNA prepared from both tumors and corresponding tail tissue of *Tyr-CreER<sup>T2</sup>:BRAF<sup>CA/+</sup>:Ppp6c<sup>flox/+</sup>* mice. (Left) Fragments of 185, 308, and 335 bp correspond to the *BRAF* WT allele, unrearranged *BRAF<sup>CA</sup>*, and *BRAF<sup>VE</sup>* alleles, respectively. (Middle) Fragments of 768 and 113 bp correspond to floxed and exon 4-deleted *Ppp6c* alleles, respectively. (Right) Fragments of 715 and 615 bp correspond to floxed and WT *Ppp6c* alleles, respectively. C, Histopathological examination of UV-induced tumors (#10 and #14 in Table 1) showing H&E staining plus Ki67 and S100 immunohistochemistry. Scale bar: 100  $\mu$ m. D, H&E staining of UV-induced tumors #10 and #14. Scale bar: 50  $\mu$ m. Arrowheads indicate tumor cells containing melanin granules

**FIGURE 3** Comparison of mutational signatures in UV-induced tumors from *Ppp6c* WT and heterozygous tumors, and identification of *Trp53* mutations. A, Pie chart showing proportion of mutational signatures seen in tumor #3 (in Table 1), which is *Ppp6c<sup>+/+</sup>* (+/+), and in tumor #13 (in Table 1), which is heterozygous for *Ppp6c* (F/+). Unknown indicates an unidentifiable signature. B, Categorical scatter plot of mutational signatures. Horizontal axis shows each signature with WT (+/+) *Ppp6c* on left and heterozygous *Ppp6c* (F/+) on right. Vertical axis indicates the proportion of signatures in each sample. \* $P < .05$ , Student t test. C, 3-D bar graph of *Trp53* mutations in samples analyzed here. Longitudinal axis indicates samples analyzed. Horizontal axis indicates *Trp53* mutations. To portray the syntenic relationship between mouse *Trp53* mutations observed here and human TP53 protein domain structure, a schematic of human TP53 protein is shown with lollipops corresponding to *Trp53* mutations observed here



the case with other variants of melanoma-like tumors listed in Table 1 (data not shown). All tumors listed in Table 1 were Ki-67-positive. These findings indicate that susceptibility to BRAF(V600E)- and UVB-induced melanoma-like tumors is greater in *Ppp6c* heterozygous relative to WT mice, and that susceptibility is greater in *Ppp6c* WT relative to homozygous mice. These findings were unanticipated, as our previous studies<sup>17-19</sup> of mouse non-melanoma skin carcinogenesis indicated carcinogenesis susceptibility descending as follows: *Ppp6c* null > *Ppp6c* heterozygous > *Ppp6c* WT mice.

### 3.2 | Exome analysis of melanoma-like tumors using next-generation sequencing

Next, we undertook exome analysis of melanoma-like tumors to compare genomic variation between tumors in *Ppp6c* WT vs heterozygous mice (Figure 3). Of 15 samples listed in Table 1, we performed total exome analysis of those whose tumor size was c. 2000 mm<sup>3</sup>, specifically, 4 samples from *Tyr-CreER<sup>T2</sup>:BRAF<sup>CA/+</sup>:Ppp6c<sup>+/+</sup>* mice and 11 from *Tyr-CreER<sup>T2</sup>:BRAF<sup>CA/+</sup>:Ppp6c<sup>flox/+</sup>* mice. Relevant histopathological analyses are summarized in Table 1, and the relationship between variant frequencies and unique variants in Figure S1. Unique variant numbers and the ratio of variant reads that reflect the tumor tissue ratio in samples showed a linear relationship, suggesting that the increase in total number of variants may be due to an increase in subclonal variants among tumors in a sample. This idea is supported by data summarized in Table 2 relevant to unique mutations. The average variant frequency was < 0.5 in both *Ppp6c* heterozygous and WT genotypes, suggesting that variant calls in this study detect somatic mutations in *Ppp6c<sup>+/+</sup>* (4 samples) and *Ppp6c<sup>flox/+</sup>* (11 samples) type tumors.

Considering variations in tumor ratio in our samples (Figure S1), we then compared quality rather than quantity of variants, namely, tumor mutation burdens, between samples. We observed a striking difference in the transition-to-transversion ratio (Ts/Tv) among genotypes. *Ppp6c<sup>+/+</sup>* tumors showed a higher Ts/Tv (5.33) than did

*Ppp6c* heterozygous tumors (3.60) (Table 2). We then compared mutational signatures<sup>37</sup> of tumor samples #3 and #13, which represent respective *Ppp6c* WT and heterozygous genotypes (Table S1). In both, Signature 7 (indicative of UV irradiation) was predominant (Figure 3A, B). Importantly, *Ppp6c* heterozygous tumors showed a significantly higher Signature 1 (mitotic clock/accumulation of DNA replication errors) ( $P = .0378$ ) than did *Ppp6c* WT tumors (Figure 3B), suggestive of a shorter cell cycle in *Ppp6c* heterozygous relative to WT tumor cells.

*TP53* mutations are frequent in human melanoma.<sup>1</sup> We found 10 different Trp53 mutations in tumors analyzed here (Table 3 and Figure 3C), and 8 corresponded to human *TP53* mutations listed in the COSMIC database (<https://doi.org/10.1093/nar/gky1015>) of human somatic mutations. The most frequent was R270C, corresponding to human R273C, which is the most frequently mutated in human cancers among the 8 described above. All 10 mouse mutations identified localized to TP53 domains are known to be important for function of human TP53, such as DNA binding and tetramerization domains, suggesting that these mutations transform TP53 into a driver of mouse melanoma-like tumors.

### 3.3 | Tumor formation by *Ppp6c* heterozygous vs null melanocyte lines, and effects of *Ppp6c* knockdown in *Ppp6c* heterozygous cells

To determine why *Ppp6c* haploinsufficiency enhances the progression of melanoma-like tumors to a greater extent than either complete loss of *Ppp6c* or the presence of WT *Ppp6c*, we undertook analysis similar to that reported in Figure 1 to establish cell lines from tumors generated in *Tyr-CreER<sup>T2</sup>:BRAF<sup>CA/+</sup>:Ppp6c<sup>+/+</sup>* and *Tyr-CreER<sup>T2</sup>:BRAF<sup>CA/+</sup>:Ppp6c<sup>flox/+</sup>* mice. We established 1 line each, UV1 (*Ppp6c<sup>flox/+</sup>*) and UV37 (*Ppp6c<sup>+/+</sup>*) (Figure S2) and confirmed their respective genotypes by PCR analysis (data not shown). We then transplanted respective lines into nude mice and monitored tumor growth. Both lines gave rise to tumors but those arising from UV1 grew faster than did those from UV37 (Figure 4A). This observation was in agreement with results of our carcinogenesis experiment (Figure 1A, B) showing that tumor development is faster in  $\Delta/+$  relative to  $+/+$  groups. Next, we observed that when cultured in vitro on feeder layers and grown in RPMI containing 5% FCS and 200 nM TPA, UV37 cells proliferated more rapidly than did UV1 cells (Figure 4B right).

Next, we assessed proliferation in vitro of *Ppp6c* knockdown UV1 and UV37 lines, using cells transfected with *Ppp6c*- or control-siRNAs. Western blot analysis conducted 3 d after transfection indicated successful PP6 knockdown in both lines (Figure 4C). PP6 knockdown essentially blocked proliferation of both UV1 and UV37 lines by day 3 (Figure 4B left and middle), at which time cells from both lines began to detach. We then analyzed both remaining adherent and detached cells for apoptosis using a caspase-3 antibody and for potential DNA damage using  $\gamma$ H2AX antibody (Figure 4C). Both knockdown lines were positive for cleaved caspase 3 and  $\gamma$ H2AX and, in both cases positivity was

**TABLE 2** Summary of unique variants in exome data

	+/+		F/+		p-value
	total	(std)	total	(std)	
Average VF	0.157	(0.0876)	0.181	(0.0666)	0.676
Total unique	573	(765)	620	(576)	0.926
INDEL	1.00	(1.22)	1.18	(1.75)	0.845
SNV	572	(764)	618	(575)	0.927
Splicing related	26.8	(40.6)	31.5	(28.7)	0.861
missense	517	(684)	553	(520)	0.935
Nonsense	27.3	(38.60)	32.2	(26.1)	0.846
Ts	470	(620)	474	(439)	0.991
Tv	101	(142)	143	(136)	0.671
Ts/Tv	5.329	(0.928)	3.60	(0.828)	0.0383

**TABLE 3** Clinical analysis of *Trp53* mutations in this study

Mouse <i>Trp53</i>	No. of samples	Human TP53	Concordance*	COSMIC90 ID	COSMIC90 cases
p.V170 M	2	p.V173 M	YES	COSV52677795	65
p.L191F	3	p.L194I	YES	COSV53623808	1
p.L191R	1	p.L194R	YES	COSV52679257	64
p.T208I	1	p.T211I	YES	COSV52665474	14
p.R210C	7	p.R213C	NO	NA	NA
p.Y231N	1	p.Y234N	YES	COSV52730114	18
p.S238F	1	p.S241F	YES	COSV52661688	128
p.R246X	3	p.R249X	NO	NA	NA
p.R270C	10	p.R273C	YES	COSV52662066	699
p.A344V	1	p.A347V	YES	COSV99037318	1

\*Both mouse and human mutations are single nucleotide changes.

greater in detached cells. These data suggest that PP6 activity is indispensable for proliferation of these melanoma cells, and when its expression drops below levels expressed in heterozygous cells, apoptosis occurs.

## 4 | DISCUSSION

One aim of this study was to determine whether *Ppp6c* acts as a melanoma suppressor in vivo in mice. To this end, we generated doubly mutant mice harboring *Braf*(V600E) plus heterozygous or homozygous mutations in *Ppp6c* triggered by tamoxifen-dependent Cre induction in melanocytes. Following UV irradiation, tumors appeared first in *Ppp6c* heterozygotes, then in *Ppp6c* WT mice, and finally in *Ppp6c* homozygotes. We confirmed recombination at the *Braf*<sup>CA</sup> allele and *Ppp6c*<sup>fl<sup>ox</sup></sup> alleles in all tumors. Based on pathological findings and positivity for the melanoma markers S100, SOX10, and HMB45, we determined that mice developed a melanoma-like tumor. We then performed next-generation sequencing exome analysis of melanoma tissues: 11 heterozygous for *Ppp6c* and 4 *Ppp6c* WT. All exhibited *Trp53* mutations. Analyses of mutation signatures also showed that most mutations seen in all tissues were associated with UV irradiation (Signature 7 mutations). Therefore, we concluded that melanocytes become tumorigenic due to combined effects of *BRAF* mutations and UV irradiation (which induces *Trp53* mutation), and that *Ppp6c* haploinsufficiency is likely to enhance this process relative to *Ppp6c* WT cells.

Our previous analysis of non-melanoma skin cancer carcinogenesis<sup>17-19</sup> and our recent data relevant to oral cancer (unpublished) indicate that *Ppp6c* null status, rather than heterozygosity, significantly accelerates tumorigenesis. Therefore, our observation here that heterozygous but not homozygous *Ppp6c* loss leads to earlier melanoma development than on a *Ppp6c* WT background is unanticipated. We also observed a greater number of Signature 1 mutations (accumulation of cell clock mutations/accumulation of DNA replication errors) in *Ppp6c* heterozygous relative to *Ppp6c* WT tumors. Specifically, *Ppp6c* heterozygous tumor cells underwent a greater

number of divisions per unit time than did cells from *Ppp6c* WT tumors. Therefore, as shown in Figure 1A, *Ppp6c* heterozygous tumors are likely to emerge more rapidly due to their shorter cell cycle. In addition, the presence of unique mutations in *Ppp6c* heterozygous tumors indicates a higher transition-to-transversion ratio than that seen in *Ppp6c* WT tumors (Table 2), possibly due to the higher C to G transversion replication errors occurring during cell division.

In 2 independent analyses, we observed only 3 *Ppp6c* null tumors in 7 mice evaluated (Figure 1A bottom) and 3 *Ppp6c* null tumors in 8 mice evaluated (Figure S2A bottom), and in both cases, tumors emerged only after prolonged irradiation. Of those, we performed exome sequencing in the 2 largest *Ppp6c* null tumors (one derived from analysis shown in Figure 1A (bottom) and the other from Figure S2A (bottom)). Neither exhibited *Trp53* mutations, and both had a lower Ts/Tv ratio than did *Ppp6c* heterozygous or WT tumors (data not shown). We concluded that, in these 2 tumors, accumulation of mutations in the presence of WT *Trp53* enabled tumor cells to remain viable even in the absence of *Ppp6c* expression.

We also asked why *Ppp6c* homozygous mutant melanoma tumors showed reduced tumor-forming capacity relative to heterozygous tumors by establishing *Ppp6c* heterozygous mutant melanoma lines. When we transfected *Ppp6c* heterozygous melanoma cells with *Ppp6c* siRNA we observed greater levels of  $\gamma$ H2AX and cleaved caspase-3 than those seen in *Ppp6c* heterozygous melanoma cells transfected with control siRNA. We propose that the *BRAF*(V600E) plus *Trp53* mutation may increase the frequency of DNA damage, leading to increased frequency of error-prone repair of DNA double-strand breaks (DSBs) via nonhomologous end-joining. Given reports that PP6 functions in homology directed repair via a DNA-PK-dependent mechanism,<sup>14</sup> it is possible that DSBs are not fully repaired in PP6-deficient conditions and that their accumulation causes cells to undergo apoptosis.

In conclusion, we found that *Ppp6c*, which has been identified as a tumor suppressor in the context of a mouse non-melanoma skin cancer model, when mutated functions in vivo as a driver of melanoma carcinogenesis.

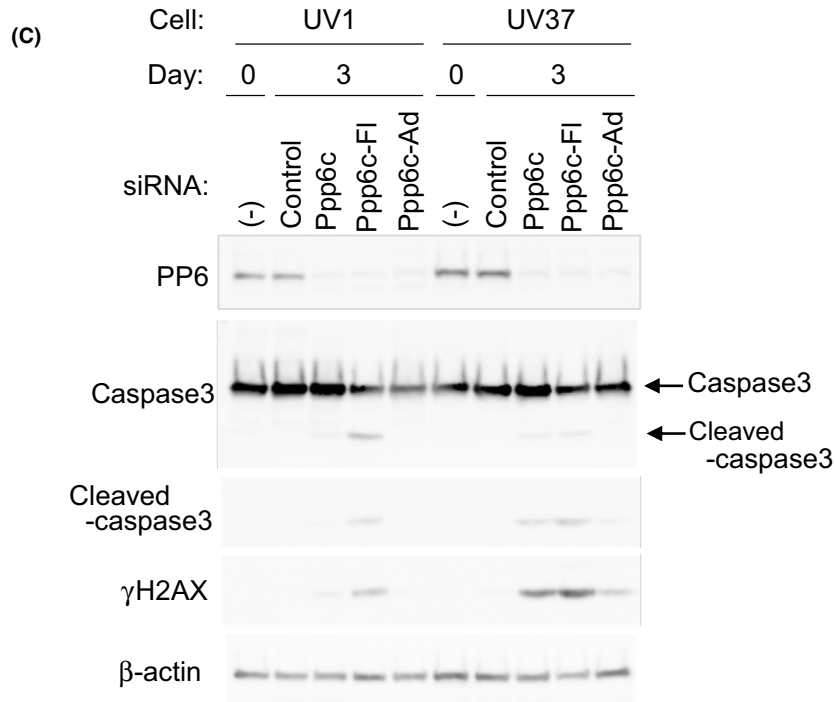
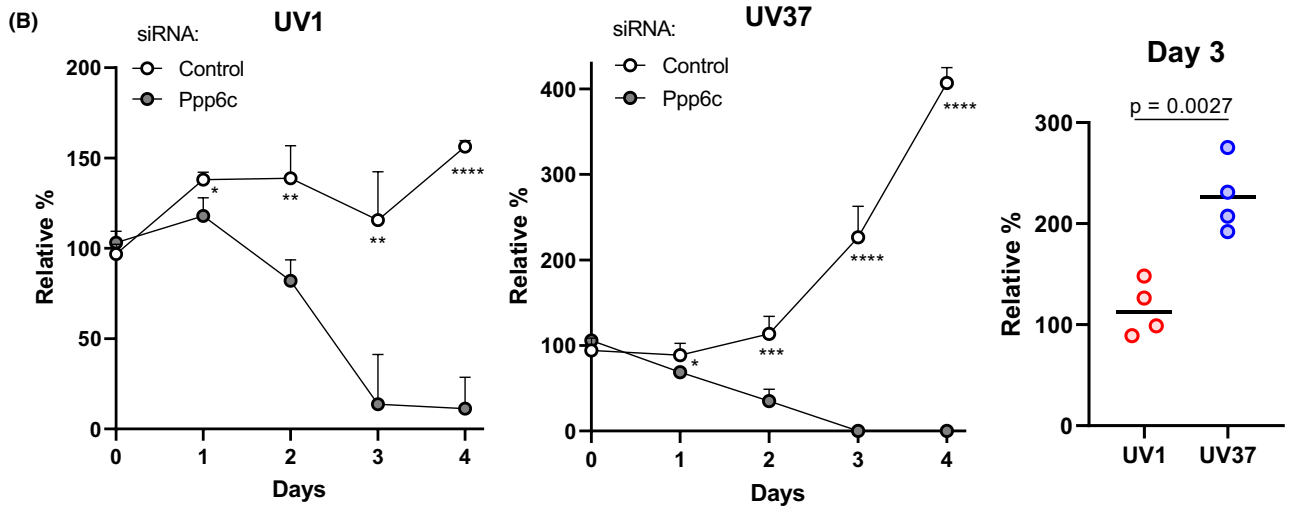
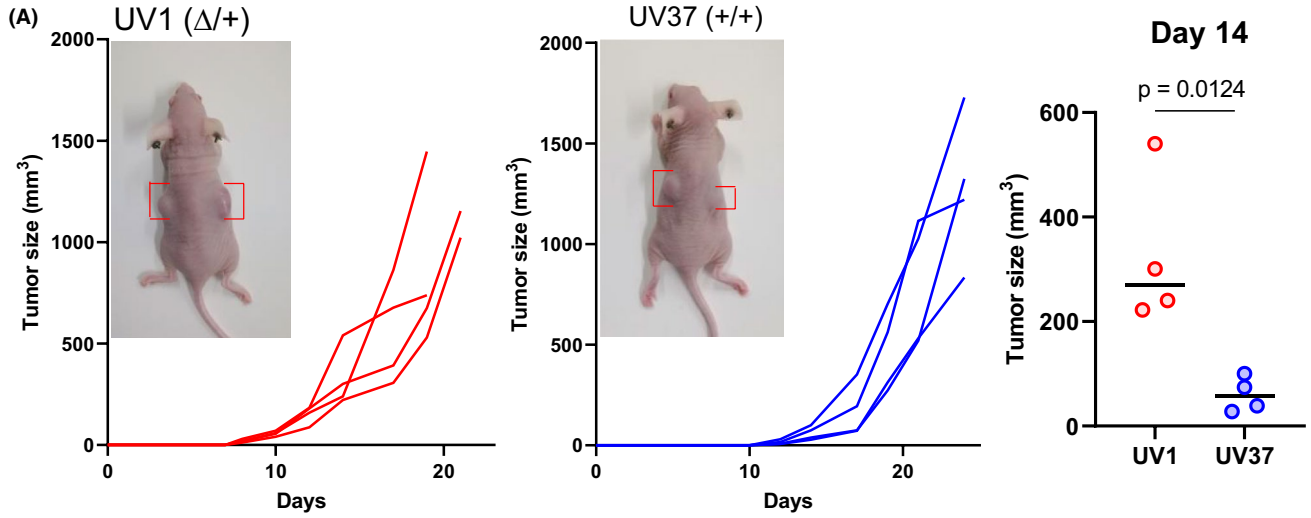


**FIGURE 4** Tumorigenicity in nude mice, and in vitro growth of melanoma cells derived from UV-induced tumors. A, Analysis following transplantation of *Ppp6c*<sup>Δ/+</sup> UV1 cells (left) or *Ppp6c*<sup>+/+</sup> UV37 cells (middle) into nude mice. Two mice were analyzed per line, and in each, a single cell line was inoculated into mice at 2 locations. Shown are changes in size of indicated tumors over time. (Right) Comparison of sizes of UV1- and UV37-derived tumors on day 14. \**P* < .05, Student *t* test. B, *Ppp6c* knockdown slows UV1 (left) and UV37 (middle) cell proliferation. Cytotoxicity and proliferation following *Ppp6c* knockdown were examined using a sulforodamine B kit:  $3 \times 10^3$  cells were seeded on feeder cells in 96-well microplates and data points were acquired over a 4-day period. Shown is the 690 nm absorbance of each sample minus absorbance of feeder cells only. The y-axis indicates the average of 4 values, with the value of living cells set at day 0 value as 100%. \*\**P* < .01, \*\*\**P* < .001, Student *t* test. (Right) Comparison of cell proliferation in UV1- and UV37-derived tumors on day 3. \*\**P* < .01 Student *t* test. C, *Ppp6c* knockdown induces apoptosis. Western blot showing levels of PP6 protein, cleaved caspase-3 (a marker of apoptosis), caspase-3 (a precursor of cleaved caspase-3),  $\gamma$ H2AX (a DNA damage marker), and  $\beta$ -actin (loading control) in control or *Ppp6c* siRNA- or control-treated UV1 (*Ppp6c* heterozygous) and UV37 (*Ppp6c* WT) cells. Also shown are analyses of floating (FI) and adherent (Ad) fractions of *Ppp6c* siRNA-treated UV1 and UV37 cells assayed at days 0 and 3 after transduction. Antibodies used and preparation of cell lysates are described in Materials and Methods

## ACKNOWLEDGMENTS

We thank Yoshimi Sakamoto and Keiko Terasaki for technical assistance. We thank Mai Oh-uchi and Yuka Chiba for secretarial assistance. We thank Dr. Elise Lamar for English editing. This work was supported by JSPS KAKENHI Grant Numbers 19K18757 to KK, 18K16043 to YI, and 17K07187 to HS.

## DISCLOSURE

The authors declare no conflict of interest.

## ORCID

Nobuhiro Tanuma  <https://orcid.org/0000-0001-7914-1380>

Hiroshi Shima  <https://orcid.org/0000-0002-0857-8929>

## REFERENCES

- Bakhoun MF, Esmaeli B. Molecular Characteristics of Uveal Melanoma: Insights from the Cancer Genome Atlas (TCGA) Project. *Cancers (Basel)*. 2019;11(8):1061.
- Hodis E, Watson IR, Kryukov GV, et al. A landscape of driver mutations in melanoma. *Cell*. 2012;150(2):251-263.
- Krauthammer M, Kong Y, Ha BH, et al. Exome sequencing identifies recurrent somatic RAC1 mutations in melanoma. *Nat Genet*. 2012;44(9):1006-1014.
- Hammond D, Zeng K, Espert A, et al. Melanoma-associated mutations in protein phosphatase 6 cause chromosome instability and DNA damage owing to dysregulated Aurora-A. *J Cell Sci*. 2013;126(Pt 15):3429-3440.
- Shi Y. Serine/threonine phosphatases: mechanism through structure. *Cell*. 2009;139(3):468-484.
- Brautigan DL. Protein Ser/Thr phosphatases—the ugly ducklings of cell signalling. *FEBS J*. 2013;280(2):324-345.
- Ohama T. The multiple functions of protein phosphatase 6. *Biochim Biophys Acta Mol Cell Res*. 2019;1866(1):74-82.
- Mi J, Dziegielewski J, Bolesta E, Brautigan DL, Larner JM. Activation of DNA-PK by ionizing radiation is mediated by protein phosphatase 6. *PLoS One*. 2009;4(2):e4395.
- Hosing AS, Valerie NC, Dziegielewski J, Brautigan DL, Larner JM. PP6 regulatory subunit R1 is bidentate anchor for targeting protein phosphatase-6 to DNA-dependent protein kinase. *J Biol Chem*. 2012;287(12):9230-9239.
- Zeng K, Bastos RN, Barr FA, Gruneberg U. Protein phosphatase 6 regulates mitotic spindle formation by controlling the T-loop phosphorylation state of Aurora A bound to its activator TPX2. *J Cell Biol*. 2010;191(7):1315-1332.
- Ziembik MA, Bender TP, Larner JM, Brautigan DL. Functions of protein phosphatase-6 in NF-kappaB signaling and in lymphocytes. *Biochem Soc Trans*. 2017;45(3):693-701.
- Stefansson B, Brautigan DL. Protein phosphatase 6 subunit with conserved Sit4-associated protein domain targets IkappaBepsilon. *J Biol Chem*. 2006;281(32):22624-22634.
- Kajino T, Ren H, Iemura S, et al. Protein phosphatase 6 down-regulates TAK1 kinase activation in the IL-1 signaling pathway. *J Biol Chem*. 2006;281(52):39891-39896.
- Zhong J, Liao J, Liu X, et al. Protein phosphatase PP6 is required for homology-directed repair of DNA double-strand breaks. *Cell Cycle*. 2011;10(9):1411-1419.
- Ghasemi M, Samaei NM, Mowla SJ, et al. Upregulation of miR-371-373 cluster, a human embryonic stem cell specific microRNA cluster, in esophageal squamous cell carcinoma. *J Cancer Res Ther*. 2018;14:S132-S137.
- Wu N, Liu X, Xu X, et al. MicroRNA-373, a new regulator of protein phosphatase 6, functions as an oncogene in hepatocellular carcinoma. *FEBS J*. 2011;278(12):2044-2054.
- Hayashi K, Momoi Y, Tanuma N, et al. Abrogation of protein phosphatase 6 promotes skin carcinogenesis induced by DMBA. *Oncogene*. 2015;34(35):4647-4655.
- Kato H, Kurosawa K, Inoue Y, et al. Loss of protein phosphatase 6 in mouse keratinocytes increases susceptibility to ultraviolet-B-induced carcinogenesis. *Cancer Lett*. 2015;365(2):223-228.
- Kurosawa K, Inoue Y, Kakugawa Y, et al. Loss of protein phosphatase 6 in mouse keratinocytes enhances K-ras<sup>G12D</sup>-driven tumor promotion. *Cancer Sci*. 2018;109(7):2178-2187.
- Dankort D, Filenova E, Collado M, et al. A new mouse model to explore the initiation, progression, and therapy of BRAF<sup>V600E</sup>-induced lung tumors. *Genes Dev*. 2007;21(4):379-384.
- Ogoh H, Tanuma N, Matsui Y, et al. The protein phosphatase 6 catalytic subunit (Ppp6c) is indispensable for proper post-implantation embryogenesis. *Mech Dev*. 2016;139:1-9.
- Elder DE, Elenitsas R, et al. Benign pigmented lesions and malignant melanoma. In: Elder DE, Elenitsas R, Rosenbach M, Murphy GF, Rubin AI, Xu X, eds. *Lever's Histopathology of the Skin, 11th edn*. Philadelphia, PA: Wolters Kluwer; 2015:853-968.
- Elder DE, Elenitsas R, Murphy GF. *Melanocytic Tumors of the Skin. AFIP Atlas of Tumor Pathology, Fourth Series, Fascicle 12*, Washington, DC, American Registry of Pathology; 2010.
- Magro CM, Crowson AN, Mihm MC. Unusual variants of malignant melanoma. *Mod Pathol*. 2006;19(Suppl 2):S41-70.
- Cheung WL, Patel RR, Leonard A, et al. Amelanotic melanoma: a detailed morphologic analysis with clinicopathologic correlation of 75 cases. *J Cutan Pathol*. 2012;39(1):33-39.
- Hong MP. Melanocytic neoplasms. In: Hoang MP, ed. *Immunohistochemistry in Diagnostic Dermatopathology*. New York, NY: Cambridge University Press; 2017:115-137.
- Soo JK, Ross AD, Bennett DC. Isolation and culture of melanoma and naevus cells and cell lines. *Methods Mol Biol*. 2011;731:141-150.
- Rosenthal R, McGranahan N, Herrero J, et al. DeconstructSigs: delineating mutational processes in single tumors distinguishes DNA repair deficiencies and patterns of carcinoma evolution. *Genome Biol*. 2016;22:17-31.

29. Robinson JT, Thorvaldsdóttir H, Winckler W, et al. Integrative genomics viewer. *Nat Biotechnol*. 2011;29(1):24-26.
30. Hinrichs AS, Karolchik D, Baertsch R, et al. The UCSC Genome Browser Database: update 2006. *Nucleic Acids Res*. 2006;1:34.
31. Wang K, Li M, Hakonarson H. ANNOVAR: functional annotation of genetic variants from high-throughput sequencing data. *Nucleic Acids Res*. 2010;38(16):e164.
32. Tate JG, Bamford S, Jubb HC, et al. COSMIC: the Catalogue Of Somatic Mutations In Cancer. *Nucleic Acids Res*. 2019;47(D1):D941-D947.
33. Gao J, Aksoy BA, Dogrusoz U, et al. Integrative analysis of complex cancer genomics and clinical profiles using the cBioPortal. *Sci Signal*. 2013;6(269):p1.
34. Cerami E, Gao J, Dogrusoz U, et al. The cBio cancer genomics portal: an open platform for exploring multidimensional cancer genomics data. *Cancer Discov*. 2012;2(5):401-404.
35. Isales MC, Mohan LS, Quan VL, et al. Distinct Genomic Patterns in Pigmented Epithelioid Melanocytoma: A Molecular and Histologic Analysis of 16 Cases. *Am J Surg Pathol*. 2019;43(4):480-488.
36. Koch MB, Shih IM, Weiss SW, et al. Microphthalmia transcription factor and melanoma cell adhesion molecule expression distinguish desmoplastic/spindle cell melanoma from morphologic mimics. *Am J Surg Pathol*. 2001;25(1):58-64.
37. Alexandrov LB, Kim J, Haradhvala NJ, et al. The repertoire of mutational signatures in human cancer. *Nature*. 2020;578(7793):94-101.

#### SUPPORTING INFORMATION

Additional supporting information may be found online in the Supporting Information section.

**How to cite this article:** Kanazawa K, Kishimoto K, Nomura M, et al. *Ppp6c* haploinsufficiency accelerates UV-induced BRAF(V600E)-initiated melanomagenesis. *Cancer Sci*. 2021;112:2233-2244. <https://doi.org/10.1111/cas.14895>